Mon. Not. R. Astron. Soc. **000**, 1–7 (2009) Printed 26 August 2009 (MN LaTeX style file v2.2)

arXiv:0908.3675v1 [astro-ph.CO] 26 Aug 2009

A Search for Neutral Carbon towards two z=4.05 Submillimetre Galaxies, GN20 and GN20.2

C. M. Casey[1]*, S. C. Chapman,[1], E. Daddi[2], H. Dannerbauer[3], A. Pope[4], D. Scott[5], F. Bertoldi[6], R. J. Beswick[7], A. W. Blain[8], P. Cox[9], R. Genzel[10], T. R. Greve[3], R. J. Ivison[11,12], T. W. B. Muxlow[7], R. Neri[9], A. Omont[13], I. Smail[14], L. J. Tacconi[10]

[1] *Institute of Astronomy, Madingley Road, Cambridge, CB3 0HA, U.K.*
[2] *Laboratoire AIM, CEA/DSM-CNRS-Université Paris Diderot, Irfu/SAp, Orme des Merisiers, F-91191 Gif-sur-Yvette, France*
[3] *MPIA, Königstuhl 17, D-69117 Heidelberg, Germany*
[4] *NOAO, 950 North Cherry Ave, Tucson, AZ 85719, U.S.A.*
[5] *Department of Physics and Astronomy, University of British Columbia, Vancouver, BC V6T 1Z1, Canada*
[6] *Argenlander Institute for Astronomy, University of Bonn, Auf dem Hügel 71, 53121 Bonn, Germany*
[7] *Jodrell Bank Centre for Astrophysics, School of Physics and Astronomy, University of Manchester, Oxford Road, Manchester, M13 9PL, U.K.*
[8] *Department of Astronomy, California Institute of Technology, 1200 E California Blvd, Pasadena, CA, 91125, U.S.A.*
[9] *Institut de Radio Astronomie Millimetrique (IRAM), St. Martin d'Heres, France*
[10] *MPE, Giessenbachstrasse 1, D-85741 Garching, Germany*
[11] *UK Astronomy Technology Centre, Royal Observatory, Blackford Hill, Edinburgh, EH9 3HJ, U.K.*
[12] *Institute for Astronomy, University of Edinburgh, Blackford Hill, Edinburgh, EH9 3HJ, U.K.*
[13] *Institut d'Astrophysique de Paris, CNRS and Université Pierre et Marie Curie, 98 Bis Boulevard Arago, 75014 Paris, France*
[14] *Institute for Computational Cosmology, Durham University, South Road, Durham DH1 3LE, U.K.*

Accepted 2009 August 7. Received 2009 August 6; in original form 2009 June 30.

ABSTRACT

Using the IRAM Plateau-de-Bure Interferometer (PdBI) we have searched for the upper fine structure line of neutral carbon ($\mathrm{C\,I}(^3P_2 \rightarrow {}^3P_1)$, $\nu_{\rm rest} = 809\,$GHz) and ^{12}CO(J=7→6) ($\nu_{\rm rest}$=806 GHz) towards the submillimetre galaxies (SMGs) GN20 (SMM J123711.9+622212, $z = 4.055$) and GN20.2 (SMM J123708.8+622202, $z = 4.051$). The far-infrared (FIR) continuum is detected at 8σ significance in GN20, with a flux density of $S_{1.8\,\rm mm} = 1.9\pm0.2\,$mJy, while no continuum is detected in GN20.2. Both sources are statistically undetected in both $\mathrm{C\,I}(^3P_2 \rightarrow {}^3P_1)$ and ^{12}CO(J=7→6) lines; we derive line luminosity limits for both C I and CO of $L' \lesssim 2\times10^{10}\,$K km s^{-1} pc^2. Assuming carbon excitation temperatures of $T_{\rm ex} = 30\,$K (the galaxies' measured dust temperatures), we infer C I mass limits of $M_{\rm CI} < 5.4\times10^6\,{\rm M}_\odot$(GN20) and $M_{\rm CI} < 6.8\times10^6\,{\rm M}_\odot$(GN20.2). The derived C I abundance limits are $< 1.8\times10^{-5}$ for GN20 and $< 3.8\times10^{-5}$ for GN20.2 implying that the systems have Milky Way level neutral carbon enrichment (X[C I]/X[H$_2$]) or lower, similar to high-redshift carbon-detected systems (at 5×10^{-5}) but about 50 times less than the neutral carbon enrichment of local starburst galaxies. Observations of GN20 and GN20.2 in high-resolution MERLIN+VLA radio maps of GOODS-N are used to further constrain the sizes and locations of active regions. We conclude that the physical gas properties of young rapidly evolving systems like GN20 and GN20.2 are likely significantly different than starburst/ULIRG environments in the local Universe yet similar to $z\sim2$ SMGs. Unless gravitationally amplified examples can be found, observations of galaxies like GN20 will require the order of magnitude increase in sensitivity of the Atacama Large Millimetre Array (ALMA) to constrain their C I and high-J CO content, despite the fact that they are the brightest systems at $z\sim4$.

Key words: galaxies: evolution – galaxies: high-redshift – galaxies: infrared – galaxies: starbursts – galaxies: individual (GN20/GN20.2)

---

* ccasey@ast.cam.ac.uk

1 INTRODUCTION

Examining the molecular gas content of distant galaxies is fundamental to our understanding of galaxy formation and evolution theories. Recent observations have shown that many distant objects contain giant molecular gas reservoirs ($> 10^{10}$ M$_\odot$; for a review see Solomon & Vanden Bout 2005). These gas repositories are thought to provide the fuel needed to power the extreme starbursts observed at high redshift through their far-IR luminosities, $L_{\rm FIR} \sim 10^{12-13}$ L$_\odot$ (e.g. Frayer et al. 1999; Neri et al. 2003; Greve et al. 2005; Tacconi et al. 2006; Chapman et al. 2008). In addition, detection of AGN in molecular gas suggests a link between the most massive starbursts, the growth of massive black holes and the onset of strong nuclear activity (Coppin et al. 2008). Molecular gas has already been detected in about 60 high redshift sources, from star forming galaxies to quasars, at redshifts $2 < z < 6.4$ (Walter et al. 2003; Bertoldi et al. 2003; Greve et al. 2005; Tacconi et al. 2006, 2008).

Carbon monoxide has bright rotational transitions and is therefore the most commonly observed tracer of molecular gas; however, CO lines are usually optically thick and difficult to model. In contrast, observations of optically thin neutral carbon (C I) can be used to derive gas physical properties without requiring detailed radiative transfer models. This is because carbon has a 3P fine-structure forming a simple, easily-analyzed three-level system. The gas excitation temperature, neutral carbon column density and mass may be derived independent of any other information provided there are detections of *both* carbon lines, C I($^3P_1 \rightarrow {}^3P_0$) (492 GHz) and C I($^3P_2 \rightarrow {}^3P_1$) (809 GHz) (e.g. Stutzki et al. 1997; Weiss et al. 2003, 2005). Furthermore, observations of either C I line could potentially be used as a probe of internal gas distribution which is independent from the more luminous optically thick CO observations.

While the Earth's atmosphere has very low transmission at the rest frequency of C I($^3P_1 \rightarrow {}^3P_0$) and is virtually opaque at C I($^3P_2 \rightarrow {}^3P_1$), some studies of neutral carbon have been performed in nearby sources where the lines are bright enough to be observed. These include the Galactic Centre, molecular clouds in the galactic disk, M82 and other nearby galaxies (e.g. White et al. 1994; Stutzki et al. 1997; Gerin & Phillips 2000; Ojha et al. 2001; Israel & Baas 2002; Schneider et al. 2003; Kramer et al. 2004). These studies show that C I and CO emission trace each other well, independent of the type of heating environment. Since they share similar critical densities, $n_{\rm cr} \sim 10^3\,{\rm cm^{-3}}$, this suggests that the C I($^3P_1 \rightarrow {}^3P_0$) and ^{12}CO($J$=1→0) transitions arise from the same gas volume and have similar excitation temperatures (Ikeda et al. 2002). In addition, several studies have found excellent agreement between C I and CO derived H$_2$ masses in local ULIRGs (e.g. Gerin & Phillips 1998; Papadopoulos & Greve 2004).

Despite improved atmospheric observing conditions at the redshifted ($z > 2$) C I frequencies, observations of distant, faint sources are particularly difficult; neutral carbon has only been confirmed previously in five other high redshift sources, three at $z \sim$2.5 (Weiss et al. 2003, 2005), one $z = 3.91$ QSO (Wagg et al. 2006) and one $z = 4.12$ QSO (Pety et al. 2004). While it is challenging to detect, C I is a cooling line and therefore is important in understanding the composition of a galaxy's dense interstellar medium (ISM). In high redshift sources, detection of C I indicates that the ISM has condensed and become significantly enriched while the Universe was still very young.

Here we report on the search for the upper fine structure line of neutral carbon, C I($^3P_2 \rightarrow {}^3P_1$), as well as the ^{12}CO(J=7→6) line, towards two of the highest redshift and most luminous submillimetre galaxies, GN20 (z = 4.055, SMM J123711.9+622212, identified in Pope et al., 2006, whose redshift was accurately measured in Daddi et al. 2009, hereafter referred to as D09) and GN20.2 (z = 4.051, SMM J123708.8+622202, also detected in ^{12}CO(J=4→3) in D09; originally from the catalogue of Chapman et al. 2001). GN20 (S_{850}=20.3 mJy) and GN20.2 (S_{850}=9.9 mJy) are two of the brightest submillimetre galaxies in GOODS-N (see also Pope 2007). Both of their rest-frame ultraviolet spectra lack any emission features (D09) and are similar to the UV spectra of many other $z \sim 2.5$ SMGs (Chapman et al. 2005). The absence of AGN characteristics in optical spectra suggests that the gas is mainly heated by star formation. Pope et al. (2006) have also shown that GN20 has a very similar SED and mid-IR spectral properties to other SMGs, as are its X-ray luminosity and photon index (cf. Alexander et al. 2005).

In addition to our interferometric millimetre observations from the Plateau de Bure Interferometer, we present high-resolution radio maps of both galaxies at 1.4 GHz from MERLIN+VLA to further characterize these bright SMGs. We organize the paper as follows: observations are described in Section 2; results are discussed in Section 3; and our discussion of the implications on high-redshift SMG enrichment are given in Section 4. Throughout, we use a Λ CDM cosmology with $H_0 = 71\,{\rm km\,s^{-1}\,Mpc^{-1}}$ and $\Omega_{\rm m} = 0.27$ (Hinshaw et al. 2009).

2 OBSERVATIONS

2.1 Molecular Line Observations

Observations were carried out with the IRAM Plateau-de-Bure interferometer through August 2008, with a 5 dish D-configuration (i.e. compact). We used the 2–mm receivers tuned to 159.873 GHz, midway between the expected redshifted frequencies of the C I($^3P_2 \rightarrow {}^3P_1$) ($\nu_{\rm rest}$ = 809.342 GHz) and ^{12}CO(J=7→6) ($\nu_{\rm rest}$ = 806.651 GHz) transitions for GN20 at $z = 4.055$ and GN20.2 at $z = 4.051$. The pointing centre was closer to GN20 than to GN20.2; since they are both off phase center, their fluxes require primary beam attenuation correction factors of 1.11 (GN20) and 2.62 (GN20.2). This observation was made possible because of the redshift measurement from the ^{12}CO(J=4→3) D09 observation. The synthesized beam size at 160 GHz is $\approx 3''$. Calibration was obtained every 12 min using the standard hot/cold–load absorber measurements. The source 3C454.3 was used for absolute flux calibration. The antenna gain was found to be consistent with the standard value of 29 Jy K^{-1} at 160 GHz. We estimate the flux density scale to be accurate to about ±15%.

Data were recorded using both polarizations overlapping, covering a 900 MHz bandwidth. The total on-source integration time was 8 hrs. The data were processed using

Table 1. Observed and Derived Properties of GN20 and GN20.2

	GN20	GN20.2
$\mathrm{RA_{MERLIN+VLA}}$ (J2000)	12:37:11.96	12:37:08.80
$\mathrm{Dec_{MERLIN+VLA}}$ (J2000)	+62:22:12.4	+62:22:01.9
$\mathrm{RA_{160}}$ (J2000)	12:37:11.89	...
$\mathrm{Dec_{160}}$ (J2000)	+62:22:12.4	...
$S_{1.4}{}^{a}$ (μJy)	73.8±12.8	170.0±12.8
$S_{\rm 3mm}{}^{a}$ (mJy)	0.33	<0.2
$S_{\rm 1.2mm}{}^{a}$ (mJy)	9.3	<2.7
$S_{\rm 1.1mm}{}^{a}$ (mJy)	11.5	...
$S_{850}{}^{a}$ (mJy)	20.3	9.9
$R_{1/2}$ MERLIN+VLA ($''$)	0.38±0.15	0.30
β	1.4 (derived)	1.5 (fixed)
L_{FIR} ($\mathrm{L_\odot}$)	1.0×10^{13}	5.0×10^{12}
$T_{\rm dust}$ (K)	30±4	30±12
$z_{\rm CO[4-3]}{}^{b}$	4.055±0.001	4.051±0.003
$I_{\rm CO[4-3]}{}^{b}$ (Jy km s^{-1})	1.5±0.2	0.9±0.3
$L'_{\rm CO[4-3]}{}^{b}$ (K km s^{-1} pc^2)	6.2×10^{10}	3.7×10^{10}
$M_{\rm H_2}{}^{b,c}$ ($\mathrm{M_\odot}$)	5.0×10^{10}	3.0×10^{10}
S_{160} Continuum (mJy)	1.9±0.2	0.5±0.3
$I_{\rm CO[7-6]} = I_{\rm CI}$ (Jy km s^{-1})^{d}	<1.2	<1.9
$L'_{\rm CO[7-6]} = L'_{\rm CI}$ (K km s^{-1} pc^2)	$< 1.6 \times 10^{10}$	$< 2.5 \times 10^{10}$
$M_{\rm H_2}$ (from CO[7-6]) ($\mathrm{M_\odot}$)	$< 1.3 \times 10^{10}$	$< 2.0 \times 10^{11}$
$M_{\rm CI}\vert_{\rm T_{ex}}$ ($\mathrm{M_\odot}$)	$< 5.4 \times 10^{6}$	$< 6.8 \times 10^{6}$
X[CI]/X[H$_2$]	$< 1.8 \times 10^{-5}$	$< 3.8 \times 10^{-5}$

Table Notes. We fit modified blackbodies to the FIR continuum flux densities (see section 3.1) to derive dust temperature and $L_{\rm FIR}$. β is reliably constrained to 1.4 for GN20 and fixed to 1.5 for GN20.2.

[a] Observed continuum flux densities from the literature at 850μm (Pope et al. 2006), 1.1mm (Perera et al. 2008), 1.2mm (Greve et al. 2008), and 3mm (D09). Upper limits for GN20.2 are 2σ. The radio flux ($S_{1.4}$) is measured at 1.4 GHz from VLA.

[b] Observed properties from D09, given here for comparison.

[c] Derived from the measured D09 CO[4-3] line strength. D09 assumes a constant brightness temperature between ^{12}CO(J=1→0) and ^{12}CO(J=4→3) to derive $\mathrm{M_{H_2}}$, but here we assume that $L'_{\rm CO[4-3]}/L'_{\rm CO[1-0]} = 8/16$ (cf. Weiss et al. 2007), and $L'_{\rm CO[7-6]}/L'_{\rm CO[1-0]} = 8/49$ (cf. Weiss et al. 2007). We also assume a conversion factor $X = \mathrm{M}_{H_2}/\mathrm{L}'_{CO} = 0.8\ \mathrm{M_\odot}$ (K km s^{-1} pc^2)$^{-1}$ (cf. Downes & Solomon 1998).

[d] Line intensity limits are 2σ. In this data, both $\mathrm{I_{CO}}$ and $\mathrm{I_{CI}}$ limits are equal since the noise measurement in each frequency range is equal, as are the assumed line widths (700 km s^{-1}).

the GILDAS packages CLIC and MAPPING and analyzed with our own IDL-based routines. The extracted data cube (2 sky coordinate axes and 1 spectral axis) has an RMS noise of 0.6 mJy. For clarity of presentation, we have re-gridded the data to a velocity resolution of ∼37 km s^{-1} (20 MHz). No obvious (>5σ) emission lines are seen in the data; however, the next section statistically tests for the presence of FIR continuum and CO and C I emission lines.

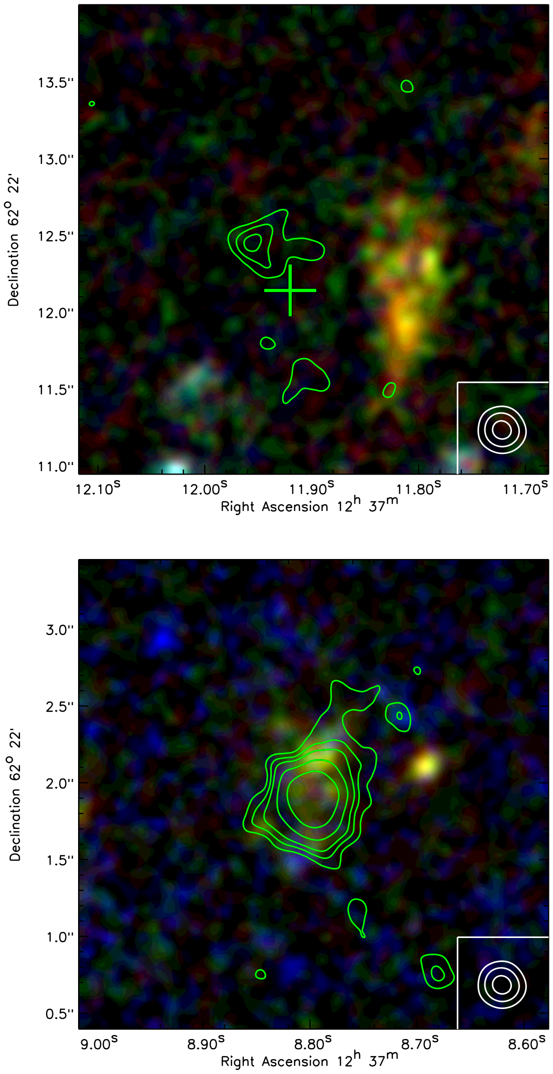

Figure 1. MERLIN+VLA radio contour overlay on *HST*/ACS *BVi* colour images of GN20 and GN20.2. The field sizes are $3'' \times 3''$ and the MERLIN beam size is $0.3''$ (outer contour of corner inset is the FWHM of the beam). The levels of the radio contours are drawn at 3, 4, 5, 7, and 10 σ; the RMS noise in the MERLIN+VLA images is 2.9 μJy and 4.6 μJy for GN20 and GN20.2 respectively. The centre of the SMA continuum emission analyzed by Iono et al. (2006) and Younger et al. (2008) is marked by the green cross on the GN20 map. The emission centroid for GN20 in the mid-IR (*Spitzer* IRAC/MIPS) is consistent with the radio and FIR continuum position. The FIR-optical offset for GN20 is significant at the 3 σ level.

2.2 MERLIN+VLA Radio Imaging

High-resolution observations from the Multi-Element Radio Linked Interferometer Network (MERLIN; Thomasson 1986) were obtained for these sources as described in Muxlow et al. (2005), with an RMS noise of ∼ 5 μJy beam^{-1}. While GN20 or GN20.2 were not imaged directly in Muxlow et al. (2005), the source is within the sensitive region of the data (Lovell Telescope primary beam). A combined MERLIN+VLA map was then constructed, with a sensitivity of 3-4 μJy beam^{-1} and high positional accuracy (tens of mas). In Figure 1, we show MERLIN radio contours on top of the *HST BVi* tricolor images (Giavalisco et al.

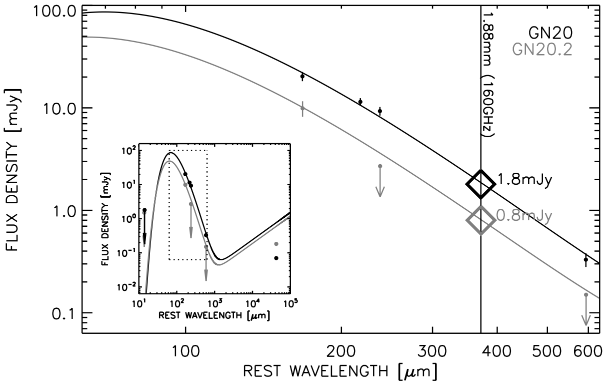

Figure 2. The SED fits to the FIR measured photometry of GN20 (black) and GN20.2 (gray). The inferred continuum flux densities at 1.88 mm are shown as large diamonds: 1.8±0.4 mJy for GN20 and 0.8±0.4 mJy for GN20.2. Their full SEDs from 10 μm near-IR to 10cm radio (rest wavelength) are shown in the inset; the area outlined in the dotted box is the zoomed-in region shown in the larger plot.

2004)[1]. The field size is 3″ × 3″ and the restoring beam size is 0.3″. We measure the center of MERLIN+VLA radio emission as 12:37:11.96, +62:22:12.4 for GN20 and 12:37:08.80, +62:22:01.9 for GN20.2.

3 RESULTS

3.1 The Continuum Contribution at 1.88mm

Interpreting the detectability and significance of emission lines in the millimetre requires an estimation of the expected continuum contribution at the wavelength of observations (160 GHz, which is a wavelength of ∼1.88 mm). Independent of our PdBI observations, we estimate the continuum flux at 1.88 mm by fitting modified-blackbody SEDs to the galaxies' FIR flux measurements. The continuum flux densities for GN20 and GN20.2 are given in Table 1. We fixed the emissivities of the galaxies to $\beta = 1.4$ for GN20 (see Pope 2007) and $\beta = 1.5$ for GN20.2 is common practice for galaxies in which β is not well constrained, although we note that letting β vary has a minimal effect, <10%, on the continuum flux). With these SED constraints we measure the dust temperatures and FIR luminosities that are given in Table 1. The SED fits to both galaxies may be seen in Fig. 2. From these fits we infer that the 1.88 mm flux generated by FIR continuum should be 1.8±0.4 mJy and 0.8±0.4 mJy for GN20 and GN20.2, respectively.

Having inferred the expected continuum level we must now *measure* the continuum from the 160 GHz PdBI observations. A 1-D spectrum for each object is first extracted at the peak integrated flux position, shown in Fig. 3. If we ignore the possible presence of emission lines, the average flux over the whole bandwidth is 1.9±0.2 mJy for GN20 and 0.5±0.3 mJy for GN20.2. The latter is consistent with the expected continuum flux, 0.8±0.4 mJy, for GN20.2, therefore we conclude that neither C I($^3P_2 \rightarrow\, ^3P_1$) nor ^{12}CO($J$=7→6) is detected in GN20.2. The GN20 average flux is consistent with the expected continuum level, 1.8 mJy, but since there is a large uncertainty in the expected flux at 1.88 mm, it needs to be further examined to see if the flux excess is due to the partial detection of C I and CO lines.

3.2 Placing limits on C I($^3P_2 \rightarrow\, ^3P_1$) and ^{12}CO($J$=7→6)

Figure 3 shows extracted 1-D spectra alongside integrated channel maps for GN20 and GN20.2. The maps are centred on each galaxy's VLA radio position, and the 1-D spectra are extracted at the point of peak integrated flux for GN20 and at the VLA centroid for GN20.2. Our observations have a ∼0.6 mJy RMS noise near GN20 and 1.6 mJy RMS noise near GN20.2across the entire 900 MHz bandwidth.

To measure the continuum without allowing contamination from possible line emission, we must extract the portion of the GN20 spectrum where line emission is anticipated. We use the measured D09 redshift and line width of ^{12}CO(J=4→3) ($z = 4.055$ and $\Delta v \sim 700\,\mathrm{km\,s^{-1}}$) as an *a priori* condition and we apply them to both ^{12}CO(J=7→6) and C I($^3P_2 \rightarrow\, ^3P_1$) lines. Unfortunately, the narrow bandwidth limits the "non-line" spectral portion to a small number of channels, specifically those with frequencies $159.75 < \nu_{\rm obs} < 159.95$ GHz or $\nu_{\rm obs} > 160.25$ GHz. We measure the continuum flux density in this spectral region to be $S_{160}(\mathrm{GN20}) = 1.4 \pm 0.3$ mJy. This suggests that a flux excess *does* exist around the expected lines, from $159.95 < \nu_{\rm obs} < 160.25$ GHz (the C I line region) and at $\nu_{\rm obs} < 159.75$ GHz (the CO line region). To test the significance of these excesses, we measure the mean flux density in each region and compare it to the "non-line" flux. The average flux density is 1.6±0.3 mJy in the C I line region and 2.5±0.4 mJy in the CO region. Both excesses are of low significance ($<2\sigma$); thus, we conclude that neither ^{12}CO(J=7→6) nor C I($^3P_2 \rightarrow\, ^3P_1$) is detected in GN20.

With no significant detection of CO or C I lines, we attribute all flux across the band to the FIR continuum, therefore the measured continuum flux densities are 1.9±0.2 mJy for GN20 and 0.5±0.3 mJy for GN20.2. The latter is consistent with no detected continuum. The former continuum measurement for GN20 is significant at the 8σ level. Although some flux from the emission lines might contribute to the flux density measurement of the continuum, we have not accounted for this additional uncertainty in our measurement.

We derive 2σ upper limits to C I and CO line intensities assuming the redshift and line width given by D09. For GN20, we measure $\mathrm{I_{CI}} \approx I_{\rm CO} < 1.2\,\mathrm{Jy\,km\,s^{-1}}$ (both limits are equal since the assumed line widths and the noise measurements in each frequency range are equal). For GN20.2, we measure $\mathrm{I_{CI}} \approx < 1.9\,\mathrm{Jy\,km\,s^{-1}}$. The corresponding limits to line luminosity are given in Table 1.

---

[1] Based on observations made with the NASA/ESA *Hubble Space Telescope*, and obtained from the Hubble Legacy Archive, which is a collaboration between the Space Telescope Science Institute (STScI/NASA), the Space Telescope European Coordinating Facility (STECF/ESA) and the Canadian Astronomy Data Centre (CADC/NRC/CSA).

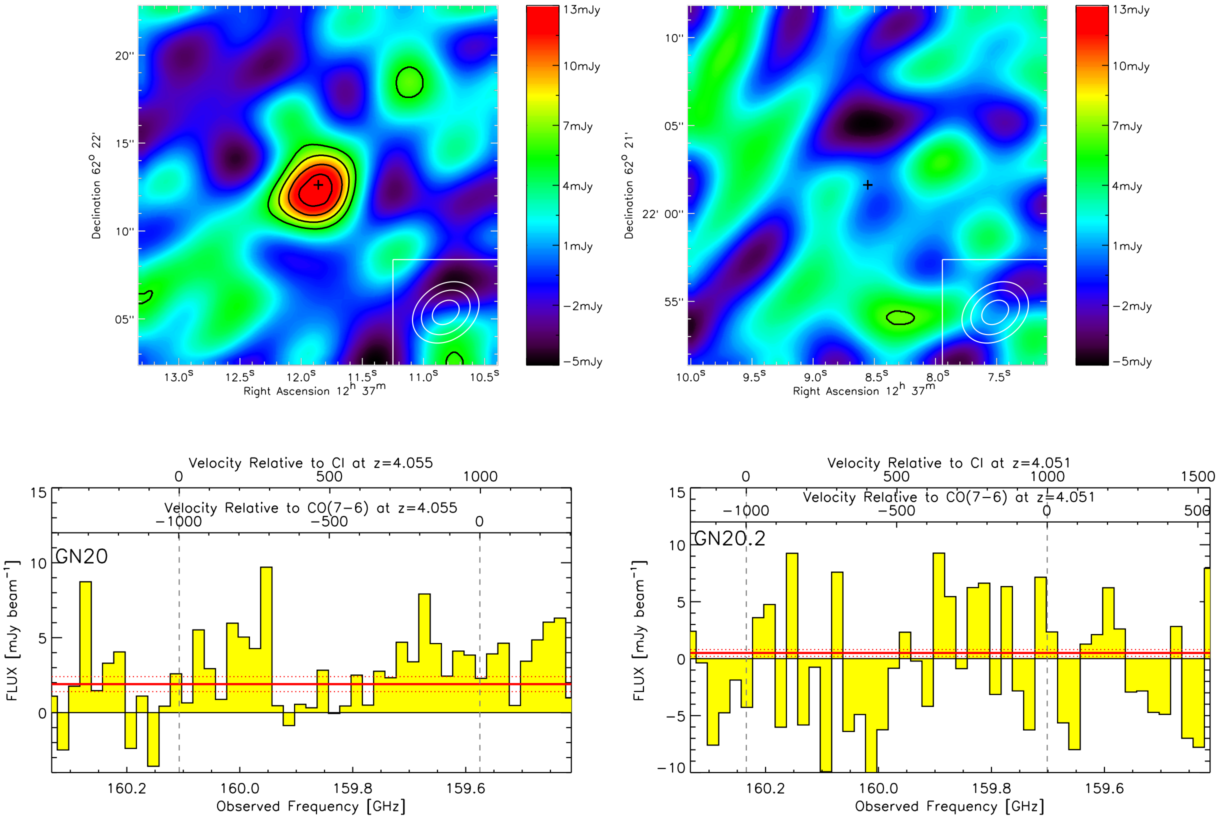

Figure 3. The 160 GHz maps and spectra for GN20 (left) and GN20.2 (right). The $20'' \times 20''$maps are integrated over the whole bandwidth; 4, 5, 6, and 7 σ contours are over-plotted (the detection of GN20 is 8 σ). The $\sim$3$''$ beam shape is shown as a lower right insert in each map. The 20 MHz spectra are extracted at the peak flux position of GN20 and at the VLA centroid position for GN20.2. The average flux, or continuum estimation in the absence of line emission, is shown as a horizontal red line bounded by 1σ uncertainties (red dotted lines). The expected frequency centres of the C I and CO emission lines (based on the D09 redshift) are marked by dashed gray vertical lines.

3.3 CO Excitation and Brightness Temperature

For interpreting CO line intensities, the assumption of constant brightness temperature has been widely taken *a priori* in the past due to lack of relevant data. However, many recent observations of multiple CO transitions in high redshift sources have shown it to be an unwarranted assumption (Dannerbauer et al. 2009). Although detailed radiative transfer models demonstrate that the ^{12}CO(J=1→0) and ^{12}CO(J=3→2) transitions are near thermal equilibrium (i.e. $L'_{\rm CO(1-0)} \approx L'_{\rm CO(3-2)}$) for the three $z \sim 2.5$ sources studied (Weiss et al. 2005), there are several AGN dominated galaxies which do not have constant brightness temperature for high-J transitions (e.g. FSC 10214+4724, APM08279+5255, and the Cloverleaf Quasar). Here we adopt the brightness temperature conversions for SMGs observed by Weiss et al. (2007), see their Figure 3; explicitly, we assume flux density ratios of $S_{\rm CO[4-3]}/S_{\rm CO[1-0]} = 10.0 \pm 0.8$ and $S_{\rm CO[7-6]}/S_{\rm CO[1-0]} = 8 \pm 1$. This implies $L'_{\rm CO[7-6]}/L'_{\rm CO[1-0]} = 8/49$ and $L'_{\rm CO[7-6]}/L'_{\rm CO[4-3]} = 64/245$. Working backwards from the D09 ^{12}CO(J=4→3) detection, this implies that ^{12}CO(J=7→6) in GN20 would have luminosity $\sim 1.6 \times 10^{10}$ K km s^{-1} pc^2. We measure a line luminosity limit of $< 1.6 \times 10^{10}$ K km s^{-1} pc^2. While there are large uncertainties in our brightness temperature conversion assumption, this measured result for GN20 agrees with the estimated population of the higher-J transitions according to other high-z SMGs. Our data for GN20.2 are less constraining due to the greater noise; our limit on line luminosity is consistent with $L'_{\rm CO[7-6]} \approx 1.2 \times 10^{10}$ K km s^{-1} pc^2, which is the expected luminosity extrapolated from the ^{12}CO(J=4→3) detection.

3.4 Radio Source Sizes

We use high-resolution MERLIN+VLA radio maps to constrain the size of the 1.4 GHz emission, to better assess the contributions from AGN and starbursts. The measurements of angular size were made using AIPS software JMFIT, deconvolving the restoring beam before attempting to derive the fitted Gaussian size. Since the signal to noise is quite low in GN20, it is impossible to detect component extensions smaller than the width of the restoring beam. Figure 1 shows the MERLIN+VLA 1.4GHz radio maps as contours on top of *HST* ACS i-band imaging. We measure the angular FWHM of the GN20 emission region to be 0.38±0.15$''$, but it is only significant above the 0.3$''$ beam size at the 2.4σ level, while the 0.5$''$ radio-optical offset is significant at the 3σ level.

Iono et al. (2006) showed that the 850 μm Smithsonian Millimeter Array (SMA) position of GN20 was significantly offset from the optical emission ($0.8''$ offset also at the 3σ level). Younger et al. (2008) obtained higher resolution continuum imaging of GN20 with the SMA and constrained the size to $0.60 \pm 0.13''$ claiming it to be partially resolved. This is consistent with our MERLIN+VLA-measured size of $0.38 \pm 0.15''$ due to the large uncertainties on both measurements. Because GN20 is not exceptionally bright in the radio (74 μJy), we cannot determine if its asymmetric, extended MERLIN+VLA morphology is significant; therefore, we cannot rule out that GN20 might be a radio point source dominated by AGN activity.

The radio source size of GN20.2 is measured to be entirely unresolved at $< 0.30''$. Radio emission with $S_{1.4} > 100\,\mu$Jy at $z = 4.051$ constrained by $R_{1/2} < 0.30''$ would have to emit at a super-Eddington rate if it were completely dominated by star formation (a calculation based on the theoretical maximum star formation density, cf. Elmegreen 1999; Casey et al. 2009). For this reason, GN20.2's radio emission is likely partially generated, if not dominated by an AGN at the galaxy's core.

4 DISCUSSION

4.1 Neutral Carbon and H$_2$ Mass

Using the formulae given in Weiss et al. (2003) for the upper fine structure line of neutral carbon C I($^3P_2 \rightarrow {}^3P_1$), we can derive the mass of neutral carbon via

$$M_{\rm CI} = C\, m_{\rm CI}\, \frac{8\pi k \nu_0^2}{hc^3 A_{10}}\, Q(T_{\rm ex})\, \frac{1}{5}\, {\rm e}^{-T_2/T_{\rm ex}}\, L'_{\rm CI(^3P_2 \rightarrow\, ^3P_1)}, \qquad (1)$$

where $Q(T_{\rm ex}) = 1 + 3{\rm e}^{-T_1/T_{\rm ex}} + 5{\rm e}^{-T_2/T_{\rm ex}}$ is the neutral carbon partition function[2]. In the equation above, $T_1 = 23.6$ K and $T_2 = 62.5$ K represent the energies above the ground state, $L'_{\rm CI(^3P_2 \rightarrow\, ^3P_1)}$ is given in K km s^{-1} pc^2, $m_{\rm CI}$ is the mass of a single carbon atom, and C is the conversion between cm^2 and pc^2, 9.5×10^{36} cm^2/pc^2. This assumes both carbon lines are in local thermodynamical equilibrium (LTE) and that C I emission is optically thin. Inserting numerical values in Equation 1 yields

$$M_{\rm CI} = 4.566 \times 10^{-4}\, Q(T_{\rm ex})\, \frac{1}{5}\, e^{-62.5/T_{\rm ex}}\, L'_{\rm CI(^3P_2 \rightarrow\, ^3P_1)} [{\rm M}_\odot]. (2)$$

Determining M$_{\rm CI}$ definitively requires measurement of the excitation temperature, which can only be done by detecting both C I($^3P_1 \rightarrow {}^3P_0$) and C I($^3P_2 \rightarrow {}^3P_1$), the two C I fine structure lines. If $T_{\rm ex}$ cannot be measured directly, it is often assumed to be equal to the characteristic dust temperature (although in the case of the Cloverleaf Quasar, Weiss et al. 2003 showed that $T_{\rm ex}$=30 K, significantly less than the dust temperature, 50 K). As the excitation temperature is unknown for both GN20 and GN20.2, we assume that $T_{\rm ex} = T_{\rm dust}$, which is appropriate, since here we are only able to derive upper limits on carbon mass for both systems. If the excitation temperature is less than the dust temperatures (like the Cloverleaf), the upper limits on carbon mass would decrease. Without accounting for the possible magnification proposed by Pope (2007), we derive upper limits on carbon mass of 5.4×10^6 M$_\odot$ (GN20) and 6.8×10^6 M$_\odot$ (GN20.2).

Table 1 also lists the limits on H$_2$ mass derived from the ^{12}CO(J=7→6) line luminosity limits, assuming brightness temperature conversions from Weiss et al. (2007). We also assume the standard ULIRG conversion factor $X = M_{\rm H_2}/L'_{\rm CO} = 0.8\,{\rm M}_\odot\ ({\rm K\,km\,s^{-1}\,pc^2})^{-1}$ (Downes & Solomon 1998).

4.2 C I Abundance in the Molecular Gas Reservoir

Neutral carbon abundance, which is independent of magnification and adopted cosmology, is estimated using the ratio of masses between C I and H$_2$ through $X[{\rm CI}]/X[{\rm H_2}] = M_{\rm CI}/(6\, M_{\rm H_2})$. We calculate a carbon abundance upper limit using the $M_{\rm H_2}$ value derived by D09. We find that $X[{\rm CI}]/X[{\rm H_2}] \lesssim 1.8 \times 10^{-5}$ for GN20 and $X[{\rm CI}]/X[{\rm H_2}] \lesssim 3.8 \times 10^{-5}$ for GN20.2. Both limits are consistent with the C I abundance in the Milky Way Galaxy, $X[{\rm CI}]/X[{\rm H_2}] = 2.2 \times 10^{-5}$ (Frerking et al. 1989), but are much lower than the measured carbon abundances of local starburst galaxies $\sim 1.5 \times 10^{-3}$ ($\sim$50 times the abundance of the MW, e.g. Schilke et al. 1993; White et al. 1994). Israel & Baas (2001) and Israel & Baas (2003) find similar carbon abundances in local ULIRGs although they account for total carbon mass instead of C I alone. In comparison, the handful of carbon abundance measurements that have been made at high redshift average to $\sim 5 \pm 3 \times 10^{-5}$ (e.g. Weiss et al. 2005; Pety et al. 2004). This is consistent with both the Milky Way's abundance and the two limits we have derived for GN20 and GN20.2. We note that an abundance near (or exceeding) that of the Milky Way implies that the cold molecular gas in GN20 or GN20.2 would already be significantly enriched 1.6 Gyrs after the Big Bang (a possibility that is not excluded by our limits). More observations of C I and CO in high redshift galaxies and QSOs are needed to investigate possible C I abundance variations with redshift or variations between differently heated environments (star formation dominant versus AGN).

5 CONCLUSIONS

GN20 has become one of the best studied high redshift starburst systems in the GOODS-N field, due to its high apparent infrared luminosity. Its diverse multiwavelength coverage has revealed very low apparent levels of AGN emission relative to its high star formation. Observations of GN20 in molecular emission lines have allowed a characterization of the system's gas properties, from the strong detection of ^{12}CO(J=4→3) of D09 to the non-detections of C I($^3P_2 \rightarrow {}^3P_1$) and ^{12}CO($J$=7→6) in this paper. We have also characterized the molecular gas of GN20.2, a nearby SMG at $z = 4.051$.

Millimetre and Sub-millimetre continuum observations suggest a continuum flux density at 160 GHz of $S_{160\,GHz} = 1.8$ mJy for GN20 and 0.8 mJy for GN20.2. We measure 1.9 ± 0.2 mJy continuum for GN20 and 0.5 ± 0.3 mJy continuum emission from GN20.2. The former is significant at the 8σ level while the latter is not statistically different from zero.

---

[2] We note that the negative sign in the exponent of $1/5\ {\rm e}^{-T_2/T_{\rm ex}}$ was accidentally omitted from the text of Weiss et al. (2003) and Weiss et al. (2005).

GN20 and GN20.2 are undetected in C I($^3P_2 \rightarrow {}^3P_1$) and ^{12}CO($J$=7→6) using observations from the IRAM-PdBI in the D-configuration at 160 GHz. Line intensity upper limits are given as $I_{\rm CO[7-6]}$(GN20)= $I_{\rm CI}$(GN20) $< 1.2\,{\rm Jy\,km\,s^{-1}}$, and $I_{\rm CO[7-6]}$(GN20.2)= $I_{\rm CI}$(GN20.2) $< 1.9\,{\rm Jy\,km\,s^{-1}}$.

High-resolution radio imaging from MERLIN+VLA show that the radio emission of GN20 is extended over $0.38\pm0.15''$ (2.7 kpc). This size is consistent with the FIR continuum size measured by Iono et al. (2006) and Younger et al. (2008). In contrast, GN20.2 is unresolved at $<0.30''$ (2.0 kpc), suggesting that AGN emission may dominate its radio emission.

The conditions for metal enrichment of the ISM of GN20 and GN20.2 do not appear to differ greatly with other high redshift sources or the Milky Way. However, local starburst galaxies have ∼50 times the carbon abundance of the high-z systems and the upper limits for GN20 and GN20.2.

Future observations from the Atacama Large Millimeter Array (ALMA) of cooling gas emission lines like C I($^3P_1 \rightarrow {}^3P_0$) and C I($^3P_2 \rightarrow {}^3P_1$) in high redshift sources will significantly advance the understanding of the relationship between early star formation and metal enrichment. Although difficult (in the absence of a boost from gravitational lensing) to observe with current instruments as evidenced by the lack of detection in GN20, one of the brightest known high redshift SMGs, C I is an excellent tracer of cold molecular gas in galaxies. It may even provide useful constraints on gas content when undetected relative to CO, and may be used as a powerful diagnostic of galaxy evolution out to the highest observable redshifts, especially in the light of the next generation of mm and submm telescopes.

ACKNOWLEDGMENTS

Based on observations carried out with the IRAM Plateau de Bure Interferometer. IRAM is supported by INSU/CNRS (France), MPG (Germany) and IGN (Spain). We acknowledge the use of GILDAS software (`http://www.iram.fr/IRAMFR/GILDAS`). CMC thanks the Gates-Cambridge Trust and IRS thanks STFC for support. ED gratefully acknowledges funding support from ANR-08-JCJC-0008.

REFERENCES

Alexander D. M., Bauer F. E., Chapman S. C., Smail I., Blain A. W., Brandt W. N., Ivison R. J., 2005, ApJ, 632, 736

Bertoldi F., et al., 2003, A&A, 409, L47

Casey C. M., Chapman S. C., Muxlow T. W. B., Beswick R. J., Alexander D. M., Conselice C. J., 2009, MNRAS, 395, 1249

Chapman S. C., Blain A. W., Smail I., Ivison R. J., 2005, ApJ, 622, 772

Chapman S. C., et al., 2008, ApJ, 689, 889

Chapman S. C., Richards E. A., Lewis G. F., Wilson G., Barger A. J., 2001, ApJL, 548, L147

Coppin K. E. K., et al., 2008, MNRAS, 389, 45

Daddi E., et al., 2009, ApJ, 694, 1517

Dannerbauer H., Daddi E., Riechers D. A., Walter F., Carilli C. L., Dickinson M., Elbaz D., Morrison G. E., 2009, ApJL, 698, L178

Downes D., Solomon P. M., 1998, ApJ, 507, 615

Elmegreen B. G., 1999, ApJ, 517, 103

Frayer D. T., et al., 1999, ApJL, 514, L13

Frerking M. A., Keene J., Blake G. A., Phillips T. G., 1989, ApJ, 344, 311

Gerin M., Phillips T. G., 1998, ApJL, 509, L17

Gerin M., Phillips T. G., 2000, ApJ, 537, 644

Giavalisco M., et al., 2004, ApJL, 600, L93

Greve T. R., et al., 2005, MNRAS, 359, 1165

Greve T. R., Pope A., Scott D., Ivison R. J., Borys C., Conselice C. J., Bertoldi F., 2008, MNRAS, 389, 1489

Hinshaw G., et al., 2009, ApJS, 180, 225

Ikeda M., Oka T., Tatematsu K., Sekimoto Y., Yamamoto S., 2002, ApJS, 139, 467

Iono D., et al., 2006, ApJL, 640, L1

Israel F. P., Baas F., 2001, A&A, 371, 433

Israel F. P., Baas F., 2002, A&A, 383, 82

Israel F. P., Baas F., 2003, A&A, 404, 495

Kramer C., Jakob H., Mookerjea B., Schneider N., Brüll M., Stutzki J., 2004, A&A, 424, 887

Muxlow T. W. B., et al., 2005, MNRAS, 358, 1159

Neri R., et al., 2003, ApJL, 597, L113

Ojha R., et al., 2001, ApJ, 548, 253

Papadopoulos P. P., Greve T. R., 2004, ApJL, 615, L29

Perera T. A., et al., 2008, MNRAS, 391, 1227

Pety J., Beelen A., Cox P., Downes D., Omont A., Bertoldi F., Carilli C. L., 2004, A&A, 428, L21

Pope A., et al., 2006, MNRAS, 370, 1185

Pope E. A., 2007, PhD Thesis, University of British Columbia, p.

Schilke P., Carlstrom J. E., Keene J., Phillips T. G., 1993, ApJL, 417, L67

Schneider N., Simon R., Kramer C., Kraemer K., Stutzki J., Mookerjea B., 2003, A&A, 406, 915

Solomon P. M., Vanden Bout P. A., 2005, ARA&A, 43, 677

Stutzki J., et al., 1997, ApJL, 477, L33

Tacconi L. J., et al., 2006, ApJ, 640, 228

Tacconi L. J., et al., 2008, ApJ, 680, 246

Thomasson P., 1986, QJRAS, 27, 413

Wagg J., Wilner D. J., Neri R., Downes D., Wiklind T., 2006, ApJ, 651, 46

Walter F., et al., 2003, Nature, 424, 406

Weiss A., Downes D., Henkel C., Walter F., 2005, A&A, 429, L25

Weiss A., Downes D., Walter F., Henkel C., 2007, in Baker A. J., Glenn J., Harris A. I., Mangum J. G., Yun M. S., eds, From Z-Machines to ALMA: (Sub)Millimeter Spectroscopy of Galaxies Vol. 375 of Astronomical Society of the Pacific Conference Series, CO Line SEDs of High-Redshift QSOs and Submm Galaxies. p. 25

Weiss A., Henkel C., Downes D., Walter F., 2003, A&A, 409, L41

White G. J., Ellison B., Claude S., Dent W. R. F., Matheson D. N., 1994, A&A, 284, L23

Younger J. D., et al., 2008, ApJ, 688, 59